Molecular Crystals and Liquid Crystals Incorporating Nonlinear Optics

Publication details, including instructions for authors and subscription information:
http://www.tandfonline.com/loi/gmcl17

ESR and ENDOR Studies of Functional LB Films

S. Kuroda [a], K. Ikegami [a] & M. Sugi [a]

[a] Electrotechnical Laboratory, Tsukuba, Ibaraki, 305, Japan

Version of record first published: 04 Oct 2006.

To cite this article: S. Kuroda , K. Ikegami & M. Sugi (1990): ESR and ENDOR Studies of Functional LB Films, Molecular Crystals and Liquid Crystals Incorporating Nonlinear Optics, 190:1, 111-132

To link to this article: http://dx.doi.org/10.1080/00268949008047837

Mol. Cryst. Liq. Cryst., 1990, Vol. 190, pp. 111–132
Reprints available directly from the publisher
Photocopying permitted by license only

Printed in the United States of America

ESR and ENDOR Studies of Functional LB Films

S. KURODA, K. IKEGAMI and M. SUGI

Electrotechnical Laboratory, Tsukuba, Ibaraki 305, Japan

Role of ESR and ENDOR spectroscopies in the characterization of functional LB films is discussed. Two illustrative examples are shown. In the first case, the detailed study of in-plane molecular orientation is discussed from the analysis of the ESR and ENDOR spectra of the stable radicals detected in LB films of a merocyanine dye. By identifying a nitrogen hyperfine structure, computer simulation of the ESR spectra yields a characteristic orientation of radicals with respect to the dipping direction of the substrate. The results strongly suggest a flow orientation of J-aggregates from which radicals may originate. The observed orientation is well described by the recent theory of flow orientation.

In the second case, study of the temperature dependence of ESR signal, in particular the spin susceptibility, is shown to provide the microscopic evidence for the development of columnar structures in conducting LB films composed of amphiphilic charge-transfer complexes.

I. INTRODUCTION

Langmuir-Blodgett (LB) technique has been attracting attention as a tool for arranging molecules into monolayer assemblies.[1,2] By choosing various kinds of functional molecules these LB films may exhibit new functions unique to the alignment of molecules in monolayers. At the same time, developed LB films may serve as a system which can exhibit new phenomena unique to their structures. To understand the mechanism of new functions or new phenomena, it is necessary to characterize microscopically the structures and electronic states of molecular aggregates formed in LB films. We discuss here the role of electron spin resonance (ESR) and electron nuclear double resonance (ENDOR) spectroscopies in such microscopic analysis. Two illustrative examples shown here are the studies carried out in Electrotechnical Laboratory. One is the ESR and ENDOR studies of merocyanine-dye LB films, in which dye molecules form J-aggregates.[3–7] The other is the ESR studies of conducting LB films composed of amphiphilic charge-transfer complexes.[8–10]

The first example is related to the analysis of molecular orientation. In the structural studies of LB films, the orientation of molecules is one of the fundamental problems. ESR spectroscopy was employed to study the molecular orientation in copper-containing LB films by studying the out-of-plane anisotropy of the spec-

tra.[11–13] In those works the tilting of the principal axis of g tensor with respect to the plane normal was determined. In addition, the existence of the in-plane preferential orientation of molecules was already pointed out in references 11 and 12. However, the spectra were measured for only one direction in the film plane and no detailed measurements and analysis of the in-plane spectra were presented.

On the other hand, we introduced the plastic substrate of polyethylene terephthalate, which can be cut to fit any desired geometry in the ESR sample cavity.[3] This enabled us to perform the first direct measurements and analysis of the in-plane ESR spectra in the LB system using LB films of a merocyanine dye diluted with arachidic acid.[4–7] This system contains high-concentration stable π-electron radicals in the dark condition, which possibly arise from an intermolecular charge transfer in J-aggregates. ESR spectra of this system contain contributions from two radical species. The deconvolution of overlapped ESR signals of these species was accomplished with the aid of ENDOR-induced ESR technique. A clear hyperfine structure due to a nitrogen necleus in the dye molecule is resolved for the in-plane spectra of one of the species, permitting the detailed analysis of the in-plane molecular orientation using an ESR spectrum simulation method. The results strongly suggested a flow orientation of J-aggregates from which radicals may originate. The observed in-plane orientation is successfully described by the recently developed theory of flow orientation during LB dipping process.[14,15] The above topic will be described in the next section. Problems of in-plane orientation in LB films are attracting increasing attention.[16]

The second example is the ESR characterization of the structure and electronic states of conducting LB films composed of amphiphilic charge transfer complexes. Temperature dependence of the ESR signals provides the microscopic evidence for the development of electrically conducting columnar structures of constituent molecules. In the case of N-docosylpyridinium-$(TCNQ)_2$ LB films, the system was shown to be REHAC (Random-Exchange Heisenberg Anitiferromagneitc Chain) system.[8,9] The concentrations of structural defects were quantitatively obtained from the temperature dependence of the spin susceptibility. In the case of $(TMTTF)_3$-(tetradecylTCNQ)$_2$ LB films, anomalous temperature dependence of the linewidth, spin susceptibility and g values suggested the occurrence of Peierls instability characteristic of one-dimensional conductor.[10] These topics will be described in section III.

II. CHARACTERIZATION OF IN-PLANE MOLECULAR ORIENTATION IN LB FILMS OF A MEROCYANINE DYE

1. J-aggregates in merocyanine-dye LB films

The chemical structure of surface-active merocyanine dyes is shown in Figure 1 as DX with X = O, S or Se. Each molecule has a donor nucleus (left-hand part of the molecule) and an acceptor nucleus (right-hand part of the molecule) connected with a conjugated chain. LB films of these dyes, diluted with arachidic acid $CH_3(CH_2)_{18}COOH$ (abbreviated as C_{20}), have been known as anisotropic photoconductors.[17,18] Among those, as-grown films of DS and DSe show a characteristic

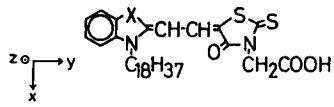

DX (X=O,SorSe)

FIGURE 1 Chemical structure of surface-active merocyanine dyes. Definition of molecular axes is also shown.

red-shifted band, J-band, in the optical absorption spectrum, indicating the formation of J-aggregates of dye molecules. Figure 2 shows a typical optical absorption spectrum of an as-grown DS film. In addition, the dissociation and restoration of J-band were shown to be controlled by the secondary treatments using heat, acid and base.[19,20] The dotted line in Figure 2 shows the spectrum after the J-band is dissociated by a heat treatment. These facts indicate the structural flexibility of J-aggregates in LB films. In fact, the degradation of orientational order of dye molecules after heat treatments were observed by the polarization dependence of optical absorption[19] or EXAFS measurements.[21] These thermo- and chemo-chromism suggest an application as optical memories.

Another interesting feature of J-aggregates in these LB films is the preferential orientation of transition dipole moment of dye molecules in the film plane, as evidenced from the in-plane optical dichroism.[19] Figure 3 shows the dependence of the optical absorption on the polarization in the film plane. The polarization vector lies in the film plane and parallel to the dipping direction of the substrate for the solid line and perpendicular to the dipping direction for the dotted line, respectively. The larger intensity of the solid line shows that the transition dipoles are preferentially oriented along the dipping direction. In Figure 1 is also shown the definition of the coordinate axes in the molecule. z-axis is parallel to the $p\pi$ orbital axis which is normal to the molecular plane. x- and y-axes are nearly parallel to the hydrophobic chain bonded to the nitrogen atom and the long axis of the

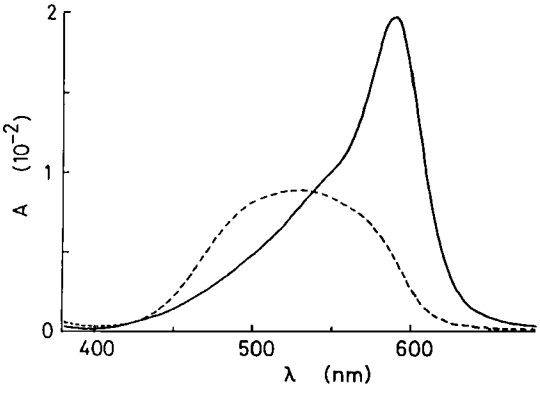

FIGURE 2 Formation of J-band in the optical absorption spectrum of an as-grown DS film (solid line) and its dissociation after heat treatment (dashed line). Ordinate shows the absorbance per monolayer (after reference 6).

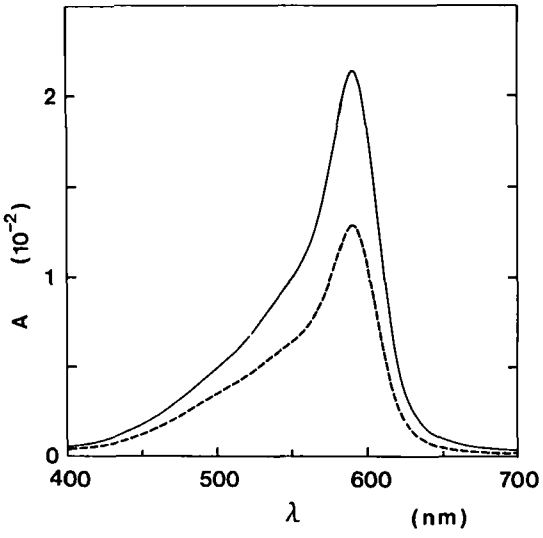

FIGURE 3 In-plane optical dichroism of a DS film. The solid and the dashed lines correspond to the electric vector parallel and perpendicular to the dipping direction, respectively (after reference 15).

chromophore, respectively. Here the chromophore shows the central portion of the molecule, consisting of conjugated chain terminated by nitrogen in the donor nucleus and the oxygen in the acceptor nucleus; N − C = C − C = C − C = O. The transition dipole moment may be nearly parallel to y-axis. From the structure of LB films it is expected that x-axis is nearly normal to the film plane, while y- and z-axis lie in the film plane. This picture is consistent with the area per molecule of 60Å^2 and the results of electro-absorption spectroscopy.[22] Thus pπ orbital axis (z-axis) becomes preferentially oriented along the direction perpendicular to the dipping direction. Such preferential orientation of the dye molecules was actually found in the anisotropy of ESR signal of this system.[4-7]

2. Stable radicals in DS LB films

While a merocyanine is diamagnetic, ESR studies of those DX LB films revealed the existence of paramagnetic species and signal enhancement by illumination.[3,4,23] The detection of photo-induced ESR signal is not surprising, if we consider that these LB films are photoconductors as pointed above. In DS LB films, however, exceptionally high-concentration stable radical species with the concentration of about 1 spin/several hundred dye molecules were detected in the dark condition.[3-7] These stable radicals are suggested to be originating from an intermolecular charge transfer in J-aggregates formed in LB films.

The solid curves in Figure 4 show the orientation dependence of the first derivative ESR spectra at X band (9.47GHz) in a DS film at room temperature with a microwave power of 2mW. The direction of the external magnetic field is normal to the film plane in Figure 4(a) whereas it lies in the film plane and makes an angle of 0°, 45°, and 90° with the dipping direction in Figures 4(b)–4(d) respectively.

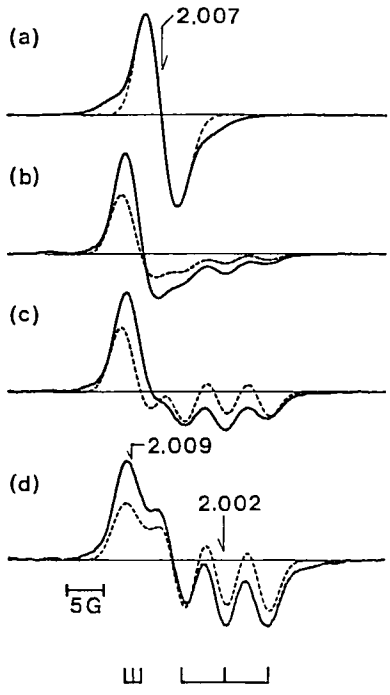

FIGURE 4 Orientation dependence of the first-derivative ESR spectra of a DS film at room temperature (solid line). The external field is normal to the film plane in (a) whereas it lies in the film plane and makes an angle of 0°, 45° and 90° with the dipping direction of the substrate for (b)–(d), respectively. The numbers show the g values of the fields as indicated. Dashed line shows the calculated spectra for radical species A. Resonance fields corresponding to the principal components of the g and the hyperfine tensors are shown at the bottom of the figure (after reference 7).

The films were deposited on a substrate of polyethylene terephthalate of 0.1 mm thick and the substrates were cut into pieces and they were stacked into the sample holder. Figures 4(b)–4(d) are the first ESR measurements of in-plane anisotropy in LB system. In-plane anisotropy is the direct evidence of the preferential orientation of radical molecules. The numbers in the figure show the g values of the field positions as indicated. These g values are close to those of π-electron radicals.

The spectra in Figure 4 in fact contain contribution of two radical species having different spin-lattice relaxation times. This can be seen from the saturation behaviour of the spectra. Figure 5(a) shows the microwave power dependence of the spectra for the external magnetic field normal to the film plane. Three curves correspond to microwave powers and temperatures of 2mW at room temperature, 0.2mW at 77K and 2mW at 77K from the lower to higher intensity at the shoulder of the spectra. Comparing these curves, it is clearly seen that there are two radical species of different linewidths. The intensity due to the species of narrower linewidth (denoted as species A, hereafter) is relatively saturated at a lower temperature compared with that of the species of wider linewidth (denoted as species B) due to the longer spin-lattice relaxation times. Since the separation of the signal of two spin species seems rather clear, the deconvolution of the ESR spectra may

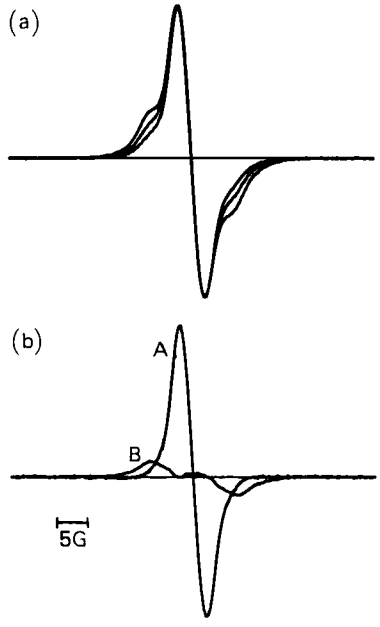

FIGURE 5 (a) Saturation behavior of the spectra for the external magnetic field normal to the film plane. Three curves correspond to microwave powers and temperatures of 2mW at room temperature, 0.2mW at 77K and 2mW at 77K from the lower to higher intensity at the shoulder of the spectra. (b) Deconvoluted spectra of radical species A and B. Refer to the text for the procedure. (Figures 5 to 9 are after reference 6).

be obtained by subtracting curves of different saturation with appropriate weight factors. For example, the signal at room temperature in Figure 5(a) is deconvoluted as in Figure 5(b).

The relative intensities of two species thus determined satisfactorily deconvolutes the ESR spectra for other external field directions, where the separation of the signals of two radical species is not so clear. Figure 6(a) shows a microwave power dependence of the spectra at 77K for the external field in the film plane and perpendicular to the dipping direction (the same direction as in Figure 4(d)). The structures tend to be washed out as signal due to species A becomes more saturated at higher microwave power levels. Figure 6(b) shows the deconvolution. The observed structures are associated with species A, while the spectra of species B is broad and structureless.

Although the above deconvolution procedure is only approximate, the obtained results were further confirmed by the selective observation of the spectra of species A by ENDOR-induced ESR measurements.[6] As reported in Reference 4, proton ENDOR signal can be detected in this system. In ENDOR-induced ESR experiments, the intensity of ENDOR signal at particular ENDOR frequency is measured as a function of the external field, giving rise to the ESR spectrum of the spin species responsible for the ENDOR response. Since ENDOR response is obtained for partially saturated species, it is likely that the spectra of species A is resolved

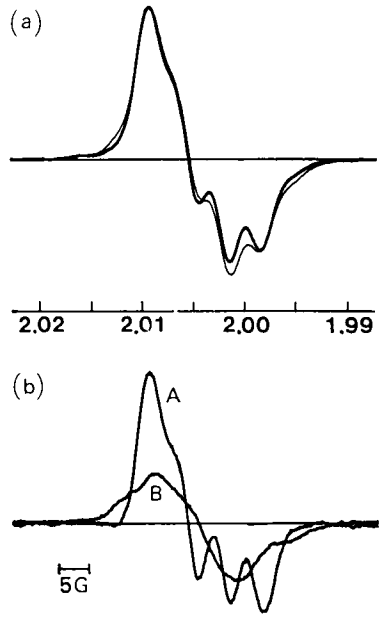

FIGURE 6 (a) Saturation behavior of the spectra at 77K for the external field in the plane and perpendicular to the dipping direction of the substrate. Microwave powers are 0.2mW for the thick-line curve and 2mW for the thin-line curve. (b) Deconvoluted spectra of species A and B.

by this method. The spectra of species B could not be saturated even at 77K. The spectra of species A were actually confirmed as seen from the comparison between the ENDOR-induced ESR spectra with the integrated form of the first-derivative ESR spectra and the deconvoluted spectra of species A in Figures 7 and 8 for the external field directions corresponding to those in Figures 5 and 6, respectively. Thus the structures of the spectra in Figure 4 are ascribed to species A.

3. Identification of nitrogen hyperfine structure for radical species A

As discussed in the section II.1, the $p\pi$ orbital axis of the dye molecule may be preferentially oriented along the direction perpendicular to the dipping direction. Figure 4(d) shows the spectrum with the external field being parallel to this direction. By comparing this spectrum with other in-plane spectra shown in Figures 4(b) and 4(c), it is noted that the triplet structure centered around the g value of 2.002 along the $p\pi$ orbital axis is most prominent in Figure 4(d). This result is consistent with a hyperfine splitting of π-electron radical with a nitrogen nucleus of spin I = 1, which shows a nearly uniaxial anisotropy with the largest magnitude of the coupling along the $p\pi$ orbital axis. In fact, there are two nitrogen sites in the molecule as seen from Figure 1 and we predicted the structure to a nitrogen hyperfine structure.[4]

To prove the triplet structure, measurement at another microwave frequency is

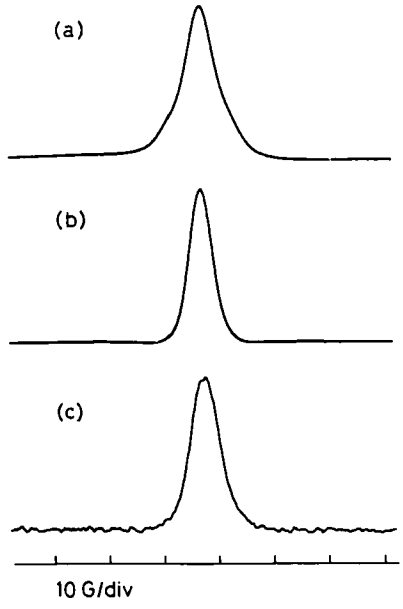

FIGURE 7 Comparison between ENDOR-induced ESR spectrum with the integrated forms of first-derivative spectra for the external field normal to the film plane. (a) Integrated form of the spectrum at 77K with microwave power of 2mW in Figure 5(a). (b) Integrated form of the deconvoluted spectrum of Species A in Figure 5(b). (c) ENDOR-induced ESR spectrum at 80K with the microwave power of 2mW. The signal was detected using proton ENDOR signal at 14.1 MHz.

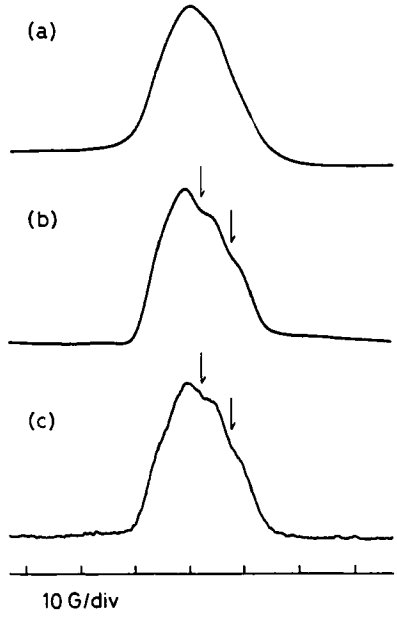

FIGURE 8 Similar comparison as Figure 7 for the external field in the plane and perpendicular to the dipping direction. (a) Integrated form of the spectrum at 77K with the microwave power of 2mW in Figure 6(a). (b) Integrated form of the deconvoluted spectrum of species A in Figure 6(b). (c) ENDOR-induced ESR spectrum at 80K with the microwave power of 2mW.

essential, because the hyperfine splitting should be independent of the frequency of measurement.[4,5] Figure 9 shows the comparison of the line shape at X-band (9.47GHz) with that at Q-band (35.0GHz) for the external field in the plane and perpendicular to the dipping direction. The results unambiguously show that the structure is the triplet structure centered at g = 2.002 as expected. On the other hand, it is seen in Figure 9 that the separation between the center of the triplet with $g = g_{\parallel}$ and the lower-field peak at $g = g_{\perp}$ increases at Q-band compared with that at X-band by the ratio of the microwave frequency (35.0/9.47). That is, the lower field peak is associated with a different g value. The situation is consistent with the distribution of the molecular axis in the plane, giving rise to the spectral turning points associated with principal g tensor components. The lower-field peak arises from the fraction of molecules with their y-axis (x- and y-axes are principal axes) pointing the external field direction, resulting in the peak at $g_y = g_{\perp}$, since $g_y > g_z$ for π-electron radicals. The triplet splitting at g_y is not resolved due to the linewidth, since the hyperfine coupling for y-axis is considerably smaller than that for z-axis. These observations establish that the main feature of the observed spectra is determined by the nitrogen coupling and the anisotropy of the observed line shape is analyzed to give the in-plane distribution of the molecular axis in the next section.

The confirmation of the nitrogen hyperfine coupling together with the identification of the observed nitrogen site were further obtained by our recent study of isotope substitution.[24] The solid line in Figure 10 shows the spectrum of a DS LB

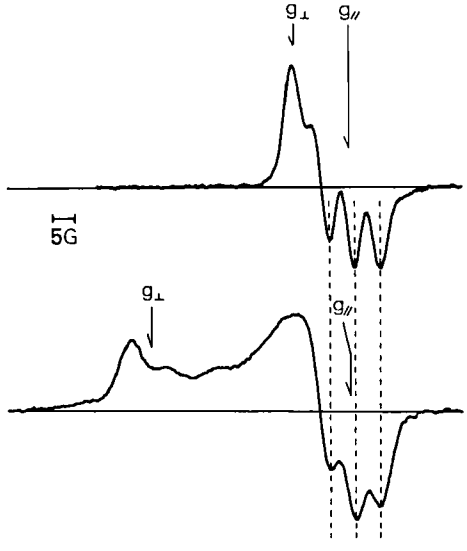

FIGURE 9 Microwave frequency dependence of the spectra in a DS film at room temperature with the external field direction in the plane and perpendicular to the dipping direction. The upper and lower curves were recorded at X- and Q-bands, respectively. Arrows indicate the field positions corresponding to $g_{\parallel} = g_z$ and $g\perp = g_y$.

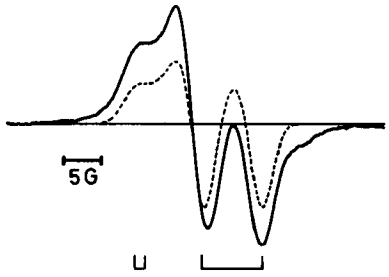

FIGURE 10 ESR spectrum in a DS film using a dye derivative with its ^{14}N nitrogen nucleus in benzothiazole being 99.7%-substituted for ^{15}N nucleus. The external field lines in the plane and perpendicular to the dipping direction. Stick lines show the hyperfine structures due to ^{15}N nucleus. Dashed line represents the calculated ESR spectrum (after reference 24).

film using a dye molecule with ^{14}N (natural abundance 99.63%) in the donor nucleus (benzothiazole in the case of DS) being 99.7% substituted by ^{15}N. The direction of external magnetic field is the same for that used in Figure 4(d). It is seen that the triplet structure in Figure 4(d) is replaced by a doublet structure in Figure 10 with the splitting 40% larger than that of the triplet as indicated by the stick lines at the bottom. This is consistent with the difference of the spin I and gyromagnetic ratio γ of the two isotopes, $I = 1$ for ^{14}N and $I = \frac{1}{2}$ for ^{15}N with the ratio of $\gamma(^{15}N)/\gamma(^{14}N) = 1.403$. The above results unambiguously show that the radical wave function is directly associated with the π-system of the dye chromophore, since the nitrogen in benzothiazole belongs to the chromophore.

4. Analysis of in-plane orientation of radical molecules

Based on the assignment of the observed structures, the ESR spectra of species A are calculated by the spectrum simulation method and the angular distribution function can be obtained.[5-7] The ESR spectrum of a π-electron radical, interacting with a nuclear spin, is well described by the following spin hamiltonian.

$$\mathcal{H} = \mu_B \mathbf{S} \cdot \mathbf{g} \cdot \mathbf{H} + \mathbf{S} \cdot \mathbf{A} \cdot \mathbf{I} \tag{1}$$

$\mathbf{g}$ in the first term (Zeeman term) and $\mathbf{A}$ in the second term (hyperfine term) represent g tensor and hyperfine tensor, respectively. We define θ as the angle between z-axis of the molecule and the dipping direction of the substrate as in Figure 11(a). The purpose of the analysis is to determine the angular distribution function of z-axis in the plane, defined as $P(\theta)$. The ESR spectrum of species A for the given direction of the external magnetic field can be calculated in the following manner. In the first step, the resonance field of the molecule of the direction given by θ is calculated from equation (1). The g value and hyperfine splitting of the given direction of the molecule, $g(\theta)$ and $A(\theta)$ are obtained as follows.

$$g^2(\theta) = g_z^2\cos^2\theta' + g_y^2\sin^2\theta'; \; A^2(\theta) = A_z^2\cos^2\theta' + A_y^2\sin^2\theta' \tag{2}$$

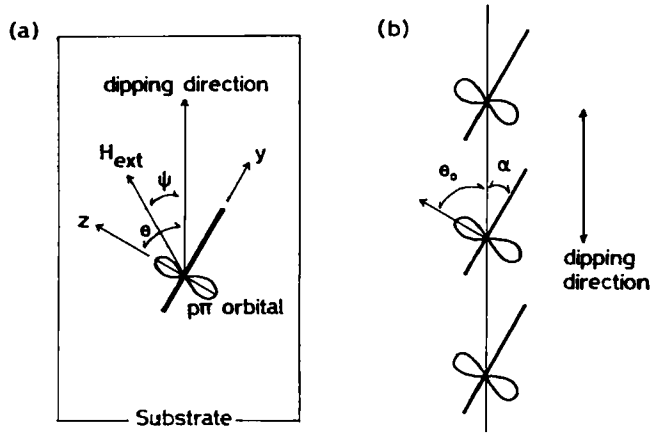

FIGURE 11 (a) Definition of angles for the calculation of the ESR spectra of species A. z- and y-axes show pπ orbital axis and the chromophore axis, respectively as in Figure 1. (b) Definition of the angle α, between the direction connecting the centers of adjacent molecules and y-axis of the molecule. θ_0 denotes the average of θ.

Here $\theta' = \theta - \psi$ is the angle between z-axis and the external field and g_i or A_i (i = y,z) show principal tensor components. The molecule of θ-direction gives the triplet signal at $g = g(\theta)$ with the triplet splitting given by $A(\theta)$. In the second step, the spectrum is obtained by summing the contribution from all directions of θ with weight factor given by $P(\theta)$. The form of $P(\theta)$ is assumed as follows.

$$P(\theta) \propto \exp(-\sin^2(\theta \pm \theta_0)/2\sin^2\delta). \quad (3)$$

Here $\pm\theta_0$ shows the most probable orientation. δ shows the width of distribution. The physical basis for the above functional form of $P(\theta)$ will be given in the next section. After calculating the spectra as functions of parameters θ_0 and δ, fairly good agreement between observed and calculated structures was obtained for $\theta_0 = 60° - 65°$ with $\delta = 25° - 30°$ as shown by dotted lines in Figures 4(b)–4(d). The apparent discrepancy that the calculated curves have smaller amplitude than observed curves is mainly due to the overlapping signals from the radical species B which has the comparable intensity with species A, as mentioned above. Strictly speaking, as will be seen in the next section, the value of δ varies according to the relative position in the substrate. This fact, however, does not significantly affects the discussion of the average orientation of radicals given below.

Figure 11(b) shows schematically the in-plane orientation of radicals with $\theta_0 = 60°$. This result shows an interesting correlation with the low-dimensional structure of J-aggregate obtained by the analysis of the shift of the J-band peak position measured from the monomeric peak position in the optical absorption spectra by Nakahara *et al.*[25] They calculated the shift as a function of the angle between the y-axis of the molecule and the direction connecting the centers of adjacent molecules, which is defined as α in Figure 11(b), using Kuhn's extended dipole model.[26] Their obtained angle was $\alpha \approx 30°$. If the direction connecting centers of adjacent

molecules of J-aggregates, or the long axis of J-aggregates in other words, is oriented along the dipping direction by a flow orientation as in the figure, the angle between the dipping direction and the z-axis of the molecule is given as $\theta_0 = 90° - \alpha \approx 60°$, which is in remarkable agreement with the angle obtained by the present analysis. This result strongly suggests that the radicals originate from the molecules forming J-aggregates and the origin of the in-plane orientation is the flow orientation.

The above shown analysis deals with only two-dimensional degree of freedom for orientation. More elaborate analysis, employing three-dimensional degree of freedom using Euler angles is also possible and the results shown in Figures 4(b)–4(d) were further confirmed.[7] In addition, the spectrum along the plane normal was analyzed as shown in dotted line in Figure 4(a), which showed that a good orientational order is present along the plane normal of the film. This is easily understood when we consider the high organization of molecules along the plane normal due to the layered structure of LB films.

5. Theory of flow orientation and its prediction

As discussed above, our ESR results are consistent with the structural model of J-aggregates oriented in the film plane due to flow orientation. Recently developed analytical model of flow orientation during LB dipping process provides the basis for quantitative understanding of the observed in-plane angular distribution function in equation (3).[14,15]

In this model, the monolayer and the substrate are approximated by a two-dimensional ideal fluid and a line sink, respectively. Flow forces acting on the molecular aggregates, elongated in shape, can be calculated from the velocity gradient tensor deduced from the complex velocity potential. The stream lines and equi-velocity potential lines obtained by this model are shown in Figure 12 by the solid and dotted lines, respectively. The actual orientation of the aggregates is

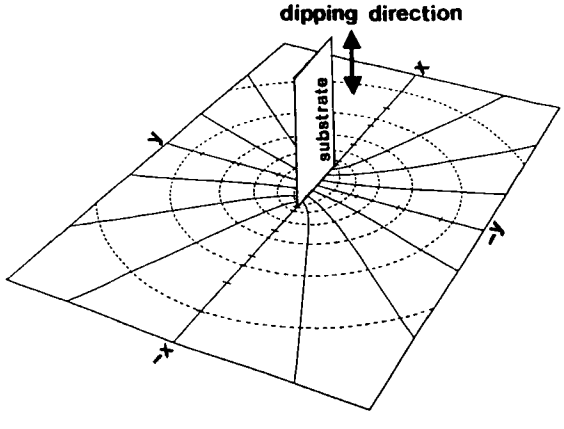

FIGURE 12 Schematic representation of the transfer process by the vertical dipping method with stream lines (solid lines) and equivelocity potential lines (dashed lines). (after reference 15).

determined from the balance between the flow force and the disturbance due to the rotatory Brownian motion, resulting in the Boltzmann distribution. If we define θ as the angle between the long axis of the aggregate and the dipping direction which is taken as y-axis in Figure 11, the angular distribution function is given as,

$$P(\theta) \propto \exp\{-(\zeta G/k_B T)\sin^2\theta\}. \quad (4)$$

Here ζ is the effective rotatory friction coefficient and G corresponds to the eigenvalue of the velocity gradient tensor. The local stress ζG is given as a sum of two terms, assuming a Bingham fluid, considering the plasticity of the monolayer;

$$\zeta G = \zeta'(4/\pi)(v_d/a)(1 - 4x^2/a^2)^{-1} + \tau_0. \quad (5)$$

The first term in the right-hand side is a Newtonian term proportional to the velocity gradient. In the first term, v_d and a show the dipping velocity and the width of substrate, respectively, and $x(-a/2 \leq x \leq a/2)$ denotes the position relative to the center of substrate along the direction perpendicular to the dipping direction. ζ' shows a Newtonian friction coefficient. The second term τ_0 is a Bingham yield value, below which the fluid behaves like an elastic body. equation (4) provides the physical basis for the observed angular distribution function in equation (3) with the parameter representing the width of distribution, $\sin^2\delta$, is given by,

$$1/2\sin^2\delta = \zeta G/k_B T. \quad (6)$$

An important conclusion from the above theory is that the degree of the orientation is dependent on the externally controllable deposition parameters of v_d and a as v_d/a, and also on the relative position in the substrate, x/a. This effect was actually confirmed for the in-plane optical dichroism of J-band.[15] Figure 13 shows the dependence of dichroic ratio R on the velocity gradient, $G = (4/\pi)(v_d/a)(1 - 4x^2/a^2)^{-1}$. R is defined as the ratio of optical absorbance with the polarization parallel to the dipping direction to that with the polarization perpendicular to the dipping direction and it can be calculated from the above theory taking the angle α in Figure 11(b) as a parameter. Closed circles in Figure 13 show the experimental points obtained from the different values of v_d, a and x. Solid line in Figure 11 shows the best fit using the above theory with the parameter values of $\zeta' = 5.0 \times 10^{-20}\text{kgm}^2\text{s}^{-1}$ and $\tau_0 = 6.2 \times 10^{-21}\text{kgm}^2\text{s}^{-2}$ in equation (5) and $\alpha = 33.5°$. These values of ζ' and τ_0 are in the reasonable range for the monolayers on the water surface and the value of α is close to the result of ESR analysis. Thus the above theory of flow orientation during LB dipping process successfully describes the dichroic behaviour of J-aggregates in DS LB films.

6. Locally resolved ESR in DS LB films

Since the stable radical species A is suggested to be originating from J-aggregates, it is interesting to see whether similar dependence of the degree of orientation on the above mentioned parameters is observed or not. From equations (5) and (6) the higher degree of orientation is expected for the higher values of (v_d/a) or toward

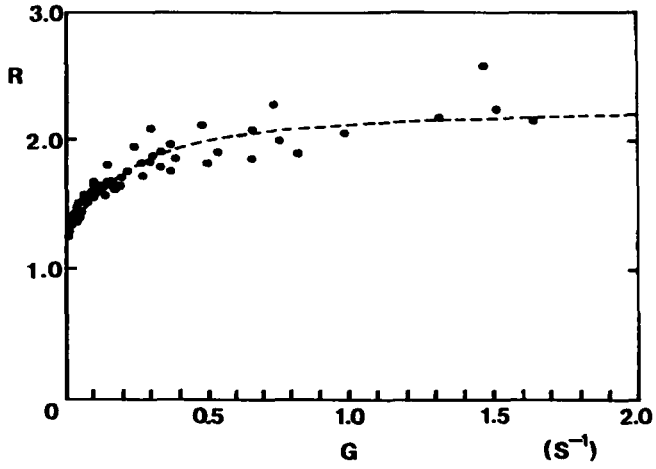

FIGURE 13 Dependence of the dichroic ratio R of the J-band on the eigenvalue G of the velocity gradient tensor. The dashed line is the best fit with $\zeta' = 5.0 \times 10^{-20}\text{kgm}^2\text{s}^{-1}$ and $\tau_0 = 6.2 \times 10^{-21}\text{kgm}^2\text{s}^{-2}$ in equation (5) and $\alpha = 33.5°$ (after reference 15).

the edge of the substrate (as x approaches to $\pm a/2$). The latter effect can be directly studied as the dependence of ESR line shape on the relative position in the substrate.[24,27] The plastic substrate can be cut into the pieces of 2mm-width according to the relative position, yielding local ESR spectra.

Solid curve in Figure 14 shows the dependence of ESR signal on the substrate position in a DS film prepared with a = 13mm and v_d = 50mm/min. The external field lines in the film plane and is perpendicular to the dipping direction. The values of x at the center of 2 mm-wide substrate are 5mm, 3mm and 1mm for the top, middle and bottom curves, respectively. Dashed curve in the figure shows the calculated ESR line shape using the local distribution function obtained from equations (3), (5) and (6). The estimated value of δ for three substrate positions of x = 1mm, 3mm and 5mm are $\delta = 26°$, 25° and 21°, respectively, using the above obtained values of ζ' and τ_0, which therefore account for the local angular distribution of the majority of molecules forming J-aggregates. As for the value of θ_0 in equation (3), fairly good agreement between observed and calculated curves was obtained for $\theta_0 \approx 58°$, which is close to the previous ESR or optical estimates mentioned above. The predicted local variation of the distribution width δ reasonably reproduces the observed line shape variation; the intensity of the resolved triplet structure increases toward the edge of the substrate, which can be recognized as the relative increase of the intensity of the shoulder marked by the arrow.

Similar results as Figure 14 were obtained for the samples prepared with different values of v_d and a. It is therefore concluded that the local orientation of radical molecules coincides well with that of the majority of molecules forming J-aggregates, which provides new evidence that the radicals have their origin in J-aggregates.

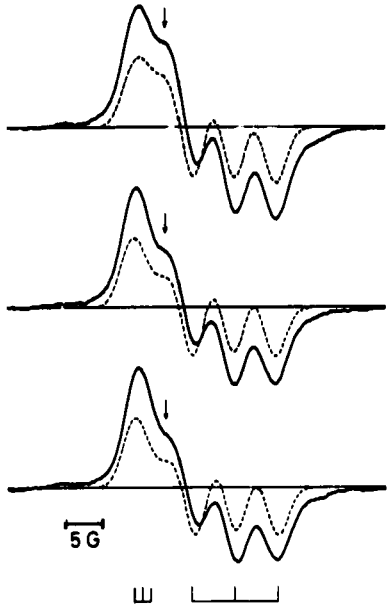

FIGURE 14 Dependence of ESR spectra on the substrate position in a DS film prepared with the substrate width a = 13mm and the dipping velocity v_d of 50 mm/min (solid curve). External field lies in the film plane and is perpendicular to the dipping direction. The values of x in equation (5) at the center of 2-mm wide piece, cut from the original substrate after deposition, are 5mm, 3mm, and 1mm for the top, middle and bottom curves, respectively. Dashed lines show calculated curves of species A using the value of δ in equation (3) theoretically estimated from equations (4) and (5) for the respective values of x. (after reference 24).

7. Discussion

So far we described the study of molecular orientation in DS LB films utilizing the ESR signal of stable radicals in some detail. The coincidence between optical and ESR in-plane anisotropies strongly suggests that the generation of stable radical species is an intrinsic phenomenon associated with J-aggregates formed in LB films.

As for the origin of the stable radicals we have proposed an intermolecular charge transfer model. As mentioned above, ESR spectra contain the signals from two radical species, A and B, of comparable spin concentration in the dark condition. Their ESR intensities seem to be simultaneously enhanced under illumination and enhanced portion decays after cutting off of illumination. These facts strongly suggest that the observed radicals are the cation and anion radicals of dye molecule generated by an intermolecular charge transfer in J-aggregates and stabilized in the molecular environment of LB films. Previous ESR confirmation of the nitrogen hyperfine coupling shows that species A is actually associated with the dye molecule. The spin density of 0.17 on the nitrogen in benzothiazole, obtained from the observed hyperfine splitting of species A provides a quantity to examine the model. This value should be consistent with the molecular orbitals of dye molecule forming J-aggregates in the charge-transferred states, if the model is correct.

On the other hand, the nature of species B is not yet clear except for its π-electron nature in the observed g values. More detailed study, concerning the ESR anisotropy and the effect of isotope substitution of relevant nuclear spin sites, would be necessary to establish that species B is also associated with the dye molecule.

There are also other observations that should be explained. The variations of spin concentration depending on the sample storage conditions are such phenomena.[3,4,6] The enhancement of ESR intensities is observed after introducing oxygen for the samples sealed under vacuum. Regardless of the pressure of ambient gas species, spin concentration increases for the first few weeks after sample deposition but subsequent variation depends on the storage conditions. ESR intensity increases for samples sealed under vacuum but gradual decrease of ESR intensity is observed for samples kept in ambient air, etc. Detailed origin of these phenomena is not known at present.

It should be emphasized, however, that despite of the existence of unexplained phenomena, the generation of these stable radical species is a new phenomenon associated with J-aggregates formed as monolayer assemblies and further studies are expected to provide deeper understanding of the nature of J-aggregates.

III. DEVELOPMENT OF CONDUCTING COLUMNAR STRUCTURES IN LB FILMS OF AMPHIPHILIC CHARGE TRANSFER COPLEXES AS EVIDENCED BY ESR

1. ESR studies of conducting LB films

ESR technique is effective in characterizing LB films composed of amphiphilic charge transfer complexes, which were introduced into LB films to construct conducting monolayer systems.[28] Barraud *et al.* reported ESR study of 1:1 complex of N-docosylpyridinium and TCNQ, before and after iodine doping.[29,30] They found that $TCNQ^-$ molecules in the precursor state are dimerized to give ESR signal of thermally excited triplet state and the orientation of the dimers was discussed from the analysis of anisotropic spectral line shape. After iodine doping, ESR spectra significantly changed, though no detailed interpretation of the results was reported. Later were developed conducting LB films composed of amphiphilic charge transfer complexes without doping by Kawabata and coworkers[31,32,33] and ESR investigation were performed on these systems.[8-10,34,35] From the temperature dependence of ESR spin susceptibility and other features, microscopic evidence was obtained for the development of conducting columnar structures of constituent molecules in a few examples. In the following, two cases of N-docosylpyridinium-$(TCNQ)_2$ LB films[8,9] and $(TMTTF)_3$-(tetradecylTCNQ)$_2$ LB films[10,35] are shown.

2. Random-Exchange Heisenberg Antiferromagnetic Chains in LB films of N-docosylpyridinium-$(TCNQ)_2$

The chemical structure of constituent molecules is shown in Figure 15. TCNQ's are in the mixed valence state, with one unpaired electron per two TCNQ mole-

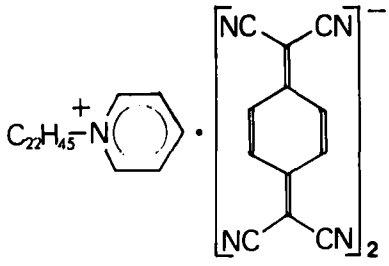

FIGURE 15 Chemical structure of N-docosylpyridinium-$(TCNQ)_2$.

cules. The conductivity of about 0.01S cm^{-1} was obtained at room temperature,[31] which suggests the development of columnar structure of TCNQ molecules. This was confirmed to be the case from the temperature dependence of spin susceptibility and its comparison with that of the powders of the same complex.

Figure 16 shows temperature dependence of the normalized spin susceptibility χ/χ_c where $\chi_c = Ng^2\mu_B{}^2S(S + 1)/3k_BT$ shows the Curie susceptibility with N being the total number of $(TCNQ)_2^-$. This quantity represents the effective number of spins at any temperature. The results show a clear crossover behaviour from one-

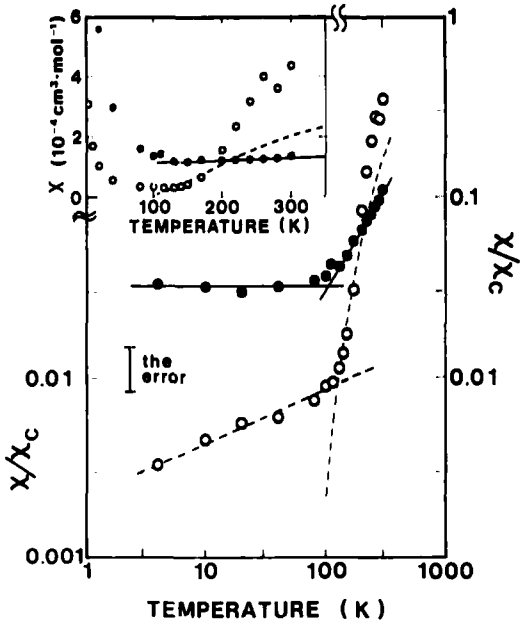

FIGURE 16 Temperature dependence of the normalized spin susceptibility of an LB film (●) and powder (○) of N-docosylpyridinium-$(TCNQ)_2$. (after reference 8 with the data of the LB film corrected as discussed in reference 9). The solid line of the higher-temperature side is the theoretical curve for the regular antiferromagnetic chain with J = 700K. The dotted line of the higher temperature side is the theoretical curve for the alternating chain with J_1 = 600K and J_2/J_1 = 0.4. The solid and the dotted lines of the lower-temperature side refer to the power laws of $\chi \propto T^{-1}$ and $\chi \propto T^{-0.7}$, respectively.

dimensional anitiferromagnetic-chain character at higher temperature to the power law at lower temperature. This behaviour is well described by the theory of Random-Exchange Heisenberg Anitiferromagnetic Chains (REHAC) developed by Soos and Bondeson. Given X_nJ being the magnitude of the random exchange between nth and (n + 1)th spins on the linear magnetic chain, where X_n ($0 \leq X_n \leq 1$) are random variables representing the disorder, they showed that the normalized bimodal distribution

$$f(X) = c\delta(\epsilon\text{-}X) + (1 - c)\delta(1 - X). \tag{7}$$

is the simplest choice for reproducing such crossover behaviour of the spin susceptibility in disordered linear chain antiferromagnet. Here c and (1-c) are the concentrations of weak exchange ϵJ and strong exchange J along the chain, respectively. For higher temperature range of $k_BT > \epsilon J$, the magnetic chains are decoupled into segments due to weak exchange (ϵJ) linkages. The susceptibility is well approximated by that of a linear chain antiferromagnet, χ_B. As the temperature is lowered, even- and odd-length segments are frozen into their ground states, singlet and doublet, respectively. A crossover takes place around the temperature given below,

$$\chi_B(T)/\chi_c \approx c/(2 - c). \tag{8}$$

where $c/(2 - c)$ is the probability for odd segments. Below this temperature the susceptibility obeys a $T^{-\alpha}(0 \leq \alpha \leq 1)$ law. It should be noted that the above situation cannot arise in two- or three-dimensional magnets, where the effect of the disorder on the spin correlation is much less significant than in the one-dimensional case.

Observed behavior of χ/χ_c at low temperatures in Figure 16 for powder (open circle) and LB films (filled circle) give $\alpha \approx 0.7$ and $c \approx 0.02$ for powder and $0.9 < \alpha < 1.0$ and $c \approx 0.07$ for LB films. Higher values of α and c shows the higher degree of disorder in LB films. From the higher temperature susceptibility, linear chain in the powder is approximated by an alternating exchange of $J_1 = 600K$ and $J_2/J_1 = 0.4$ while a uniform exchange of $J = 700K$ was suggested for LB films. This suggests the tighter stacking of molecules in the flexible structure of LB films.

The significance of the present study is that it first microscopically confirmed the development of one-dimensional stacks of TCNQ molecules in conducting LB films of charge transfer complexes and it provided the first quantitative estimation of the concentration of defects, which are presumably associated with misorientations of molecules.

3. Possible occurrence of Peierls instability in LB films of $(TMTTF)_3(tetradecylTCNQ)_2$

The chemical structure of the molecules is shown in Figure 17. This system showed a considerably high conductivity of about 1S cm^{-1} at room temperature.[33] ESR studies in this system revealed a characteristic anomaly in the temperature dependence of the signal. Figure 18(a) shows a temperature dependence of the spin

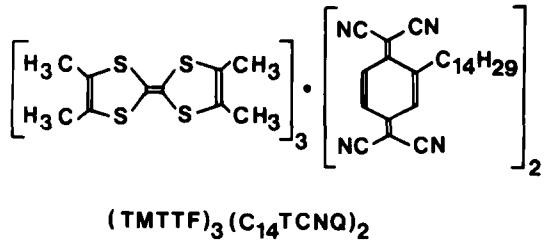

$(TMTTF)_3(C_{14}TCNQ)_2$

FIGURE 17 Chemical structure of $(TMTTF)_3(C_{14}TCNQ)_2$.

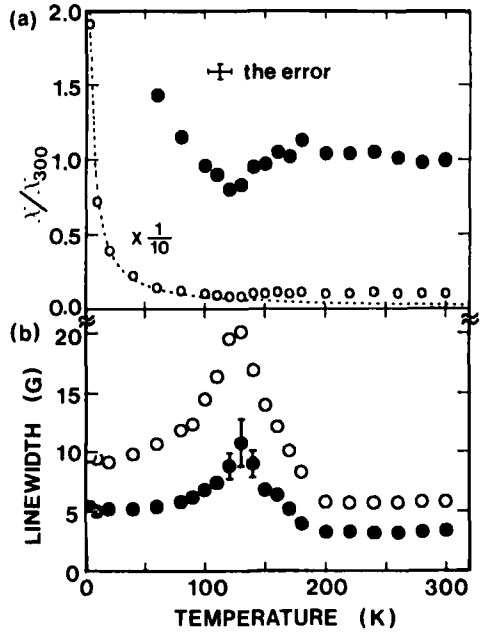

FIGURE 18 (a) Temperature dependence of spin susceptibility in an LB film of $(TMTTF)_3(C_{14}TCNQ)_2$. Dotted line refers to a Curie-like (1/T) law. (b) Temperature dependence of peak to peak line width (●) and full width at half maximum of the integrated signal (○).

susceptibility normalized by the value at 300K. The temperature dependence of the linewidth is shown in Figure 18(b). Figure 19 shows an example of the temperature dependence of ESR line shape with the external field normal to the film plane. It is seen that the linewidth shows an anomalous broadening around 130K. Corresponding to its anomaly around 130K is observed a decrease of the spin susceptibility. g value was also found to show anomalous maximum around the same temperature range. These anomalies of the spin susceptibility, linewidth and g value are analogous to those observed in the TTF-TCNQ crystal around its Peierls transition.

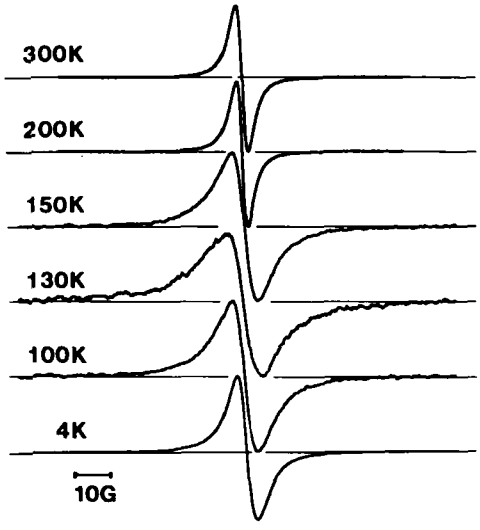

FIGURE 19 ESR signals observed for an LB film of $(TMTTF)_3(C_{14}TCNQ)_2$ at various temperatures with the external magnetic field normal to the film plane.

In the crystalline system the decrease of susceptibility and the increase of g value can be understood by the rapid decrease of the contribution from TCNQ stacks due to CDW formation. Line broadening may reflect critical fluctuation around the transition temperature. Unlike the crystalline system, the present LB film system exhibits a much higher concentration of structural defects as seen from the Curie-like susceptibility dominating at lower temperatures. Thus a distinct phase transition may not be occurring because of this large concentration of disorders. Nevertheless the above observation suggests the occurrence of Peierls fluctuation, characteristic of one-dimensional conductor. If this is true, the present observation indicates microscopically the formation of organic metal systems in LB films.

At present, other direct evidence supporting the above interpretation is not yet obtained either from structural studies or conductivity studies. Recently the above anomaly was found to be reversibly affected by the pressure of the atmosphere under which the LB films are sealed.[35] Anomaly appears at 1 atm but it becomes less distinct as the pressure is lowered. This phenomenon may be related to the flexible layered structure of LB films, affected by the pressure. Structural evidence for such flexibility may be obtained in future studies.

4. Discussion

Above shown ESR studies provided first microscopic measurements, supporting the formation of columnar structures of constituent molecules in conducting LB films composed of amphiphilic charge transfer complexes. Recently, first macroscopically metallic LB film system was developed employing alkyl ammonium and $Au(dmit)_2$ complex.[36] A high conductivity was found to be retained down to 10K. Although ESR signal of conduction electrons could not be detected, presumably

due to shorter relaxation times due to large spin-orbit coupling arising from heavy metal atom (Au) in the complex, low temperature Curie spins was certainly smaller than those of previous conducting LB films, reflecting the lower disorder and/or the higher dimensionality of this system.[37] This is consistent with the higher conductivity of $Au(dmit)_2$ system.

IV. CONCLUDING REMARKS

As we have discussed in the above two examples of dye LB films and conducting LB films, ESR and ENDOR spectroscopies provide unique structural information as well as the informations concerning electronic or magnetic states. In the isolated spins like dilute organic radicals, g value and hyperfine interaction is a rich source of information. In the case of merocyanine LB films, the anisotropy of g value and hyperfine coupling played an essential role in revealing the detailed angular distribution. In the concentrated spin system, temperature dependence of ESR signal, in particular the spin susceptibility provide important informations about electronic and magnetic phases and their transitions.

Although the discussions were not made here, the anisotropy of g value and linewidth provide important information about the molecular orientation also in concentrated spin cases. Such analyses are now in progress, for example, for pyridinium$(TCNQ)_2$ LB films.

All of the examples discussed in the present paper utilize conventional cw ESR detection. Alternative detection schemes are pulsed ESR and optically detected ESR, which may be also useful for LB films. The unpaired electrons in organic molecular aggregates involve important physics such as dark and photo-induced charge transfer, mixed valence, magnetism, structural defects, as discussed here, and also local structural transformation like soliton in polyacetylene,[38] of which wavefunction was confirmed by ESR and ENDOR spectroscopies.[39,40] Considering these points, there may be more cases where ESR and ENDOR spectroscopies will play an essential role in the understanding of functional LB films.

Acknowledgment

The present authors express their gratitude to Dr. J. Kondo for valuable discussion. They are also indebted to the colleagues in Electrotechnical Laboratory. Thanks are due to Dr. Y. Kawabata and his colleagues and Professor G. Saito for helpful discussions. Dr. S. Yasui is appreciated for the synthesis of merocyanine dyes.

References

1. H. Kuhn, D. Möbius and H. Bücher, In Techniques of Chemistry, edited by A. Weissberger and B. W. Rossiter (Wiley, New York, 1973), Vol. 1, Pt. IIIB.
2. M. Sugi, *J. Mol. Electron.*, **1**, 3 (1985).
3. S. Kuroda, M. Sugi and S. Iizima, *Thin Solid Films*, **99**, 21 (1983).
4. S. Kuroda, M. Sugi and S. Iizima, *Thin Solid Films*, **133**, 189 (1985).
5. S. Kuroda, K. Ikegami, M. Sugi and S. Iizima, *Solid State Commun.*, **58**, 493 (1986).

6. S. Kuroda, K. Ikegami, K. Saito, M. Saito and M. Sugi, *J. Phys. Soc. Jpn.*, **56**, 3319 (1987).
7. S. Kuroda, K. Ikegami, K. Saito, M. Saito and M. Sugi, *Thin Solid Films*, **159**, 285 (1988).
8. K. Ikegami, S. Kuroda, M. Saito, K. Saito, M. Sugi, T. Nakamura, M. Matsumoto and Y. Kawabata, *Phys. Rev.*, **B35**, 3667 (1987).
9. K. Ikegami, S. Kuroda, M. Saito, K. Saito, M. Sugi, T. Nakamura, M. Matsumoto, and Y. Kawabata, *Thin Solid Films*, **160**, 139 (1988).
10. K. Ikegami, S. Kuroda, K. Saito, M. Saito, M. Sugi, T. Nakamura, M. Matsumoto, Y. Kawabata and G. Saito, *Synth. Met.*, **27**, B587 (1988).
11. J. Messier and G. Marc, *J. Phys. (France)*, **32**, 799 (1971).
12. P. A. Chollet, *J. Phys.*, **C7**, 4127 (1974).
13. M. Vandevyver, A. Barraud, Ruaudel-Teixier, P. Maillard and C. Gianotti, *J. Colloid & Interface Sci.*, **85**, 571 (1982).
14. N. Minari, K. Ikegami, S. Kuroda, K. Saito, M. Saito and M. Sugi, *Solid State Commun.*, **65**, 1259 (1988).
15. N. Minari, K. Ikegami, S. Kuroda, K. Saito, M. Saito and M. Sugi, *J. Phys. Soc. Jpn.*, **58**, 222 (1989).
16. See for example, Proc. 4th Int. Conf. of LB Films, Tsukuba, 1989, Thin Solid Films, **178–180** (1989).
17. M. Sugi and S. Iizima, *Thin Solid Films*, **68**, 199 (1980).
18. M. Sugi, M. Saito, T. Fukui and S. Iizima, *Thin Solid Films*, **99**, 17 (1989).
19. T. Fukui, M. Saito, M. Sugi and S. Iizima, *Thin Solid Films*, **109**, 247 (1983).
20. M. Sugi, M. Saito, T. Fukui and S. Iizima, *Thin Solid Films*, **129**, 15 (1983).
21. H. Oyanagi, M. Sugi, S. Kuroda, S. Iizima, T. Ishiguro and T. Matsushita, *Thin Solid Films*, **133**, 181 (1985).
22. S. Nishikawa, Y. Tokura, T. Koda and K. Iriyama, *Jpn. J. Appl. Phys.*, **25**, L701 (1986).
23. T. Iwasaki, H. Wakabayashi, T. Ishii and K. Iriyama, *Appl. Phys. Lett.*, **45**, 1089 (1984).
24. S. Kuroda, K. Ikegami, K. Saito, M. Saito and M. Sugi, *Solid State Commun.*, **71**, 333 (1989).
25. H. Nakahara, K. Fukuda, D. Möbius and H. Kuhn, *J. Phys. Chem.*, **90**, 6144 (1986).
26. V. Czikkely, H. D. Försterling and H. Kuhn, *Chem. Phys. Lett.*, **6**, 11, 207 (1970).
27. S. Kuroda, K. Ikegami, K. Saito, M. Saito and M. Sugi, Thin Solid Films, **178**, 555 (1989).
28. A. Ruaudel-Teixier, M. Vandevyver and A. Barraud, *Mol. Cryst. Liq. Cryst.*, **120**, 3129 (1985).
29. A. Barraud, P. Lesieur, J. Richard A. Ruaudel-Teixier and M. Vandevyver, *Thin Solid Films*, **133**, 125 (1985).
30. J. Richard, M. Vandevyver, P. Lesieur, A. Ruaudel-Teixier and A. Barraud, *J. Chem. Phys.*, **86**, 2428 (1987).
31. T. Nakamura, M. Matsumoto, F. Takei, M. Tanaka, T. Sekiguchi, E. Manda and Y. Kawabata, *Chem. Lett.* **1986**, 709 (1986).
32. Y. Kawabata, T. Nakamura, M. Matsumoto, M. Tanaka, T. Sekiguchi, H. Komizu, E. Manda and G. Saito, *Synth. Met.*, **19**, 663 (1987).
33. M. Matsumoto, T. Nakamura, E. Manda, Y. Kawabata, K. Ikegami, S. Kuroda, M. Sugi and G. Saito, *Thin Solid Films*, **160**, 61 (1988).
34. K. Ikegami, S. Kuroda, M. Sugi, M. Saito, S. Iizima, T. Nakamura, M. Matsumoto, Y. Kawabata, and G. Saito, *Synth. Met.* **19**, 675 (1987).
35. K. Ikegami, S. Kuroda, K. Saito, M. Saito, M. Sugi, T. Nakamura, M. Matsumoto, Y. Kawabata and G. Saito, Thin Solid Films, **179**, 177 (1989).
36. T. Nakamura, K. Kojima, M. Matsumoto, H. Tachibana, M. Tanaka, E. Manda, and Y. Kawabata, *Chem. Lett.*, **1989**, 369 (1989).
37. K. Ikegami, S, Kuroda, K. Saito, M. Saito, M. Sugi, T. Nakamura, H. Tachibana, M. Matsumoto and Y. Kawabata, Thin Solid Films, **179**, 245 (1989).
38. A. J. Heeger, S. Kivelson, J. R. Schrieffer and W. P. Su, *Rev. Mod. Phys.*, **60**, 781 (1988).
39. S. Kuroda, H. Bando and H. Shirakawa, *J. Phys. Soc. Jpn.*, **54**, 3956 (1985).
40. S. Kuroda and H. Shirakawa, *Phys. Rev.*, **B35**, 9380 (1987).